



A combination of two swords thermo-bluelight-synergistic-catalytic CO₂ cycloaddition on ZnIn₂S₄ exposed abundant of Zinc cation sites

Yuning Wu^a, Xue-Fang Yu^{b,*}, Yujie Du^a, Linhong Xia^a, Qi Guo^a, Kaisheng Zhang^c,
Weilong Zhang^a, Senmiao Liu^a, Yanhua Peng^a, Zhuo Li^a, Xiaolong Yang^{a,*}

^a School of Chemistry and Chemical Engineering, State Key Laboratory of Bio-fibers and Eco-textiles, Collaborative Innovation Center of Shandong Marine Bio-based Fibers and Ecological textiles, Qingdao University, 308 NingXia Road, Qingdao 266071, PR China

^b The Laboratory of Theoretical and Computational Chemistry, School of Chemistry and Chemical Engineering, Yantai University, No. 32 Qingquan Road, Yantai 264005, PR China

^c Environmental Materials and Pollution Control Laboratory, Institute of Solid State Physics, HFIPS, Chinese Academy of Sciences, Hefei 230031, PR China

ARTICLE INFO

Keywords:

CO₂ cycloaddition
Cyclic carbonate
ZnIn₂S₄
Surface zinc sites
Thermo-photo-synergistic catalysis
Electron-rich transition state

ABSTRACT

CO₂ cycloaddition is an effective way to realize carbon neutralization. It is a great challenge to develop efficient and green catalytic system. In this work, ZnIn₂S₄ catalyst with highly exposed surface zinc sites were fabricated for thermal & blue LED driven solvent-free CO₂ cycloaddition. The optimized ZnIn₂S₄ shows efficient yield of CO₂ cycloaddition with epoxides under blue LED irradiation at 80 °C with TBAB as cocatalyst (Con 92.3%; Sel >99%; 137.1 mmol/g/h). Excellent stability and broad substrates scope was confirmed. The photoinduced hole facilitates the coordination and polarization of adsorbed propylene oxide. Simultaneously, photoinduced electron would transfer to propylene oxide molecule to form electron-rich transition state, which was not only facilitate to the open-ring step of propylene oxide, but also greatly help the activation of CO₂ adsorbed adjacent S²⁻ sites. To our knowledge, this is the first report on thermo-photo-synergistic catalytic CO₂ cycloaddition on ZnIn₂S₄.

1. Introduction

So far, fossil fuels are still the core carrier of human access to energy. The global energy consumption exceeds 10¹⁸ J in 2021, of which ~85% is provided by fossil fuels [1]. The resulted excessive carbon dioxide (CO₂) emission (concentration increasing from the preindustrial 280–417.73 ppm on January 1 2022) brings extreme weather, greenhouse effect, polar ice cap melting and ocean acidification, etc [2].

On one hand, nowadays the net-zero scenario is proposed to decrease 95% of CO₂ emission till the next 30 years, the global temperature rise is limited to less than 1.5 °C [1]. On the other hand, CO₂ is valuable C1 resource although it is difficult for activation (750 kJ·mol⁻¹). Various kinds of CO₂ utilizations technique emerge like CO₂ hydrogenation, reduction and cycloaddition to highly-added valuable fuel like methane, syngas, methanol, CO, formic acid and others [3–5]. Among these explorations, CO₂ cycloaddition reaction with an 100% atom-economy attracts intensive research interests since the pioneering work of Inoue and co-workers reported in 1969 [6], resulting cyclic carbonates is excellent Li-ion battery electrolytes, polycarbonates synthesis

monomers and pharmaceutical intermediates, etc. It was commercialized by Bayer and Mitsubishi with tetraethylammonium bromide (Et₄NBr) and tetrabutyl phosphonium iodide as catalysts, respectively [7].

Actually, various conventional thermal-catalytic systems have been explored like homogeneous catalysts (Salen Complexes, ZnCl₂/TBAB, organocatalysts) and heterogeneous catalysts (Immobilized Salen Complexes, Porphyrin-based Organic Polymers, MOFs, ZnO) [8]. Considering the current petrochemical energy shortage environment, sunlight may be inexhaustible clean energy for mankind. The solar-driven carbon recycling has been greatly developed. CO₂ was converted directly to various valuable fuels (CO, CH₄, CH₃OH, HCOOH, C₂ + ethylene, ethane, propane, ethanol) and high value-added chemicals with the help of sunlight [9–11]. In the past decade, solar-driven CO₂ cycloaddition (CCA) in whole or in part has either been greatly developed. Jiang et al. [12] synthesized Zn single-atom/hollow porous carbons catalysts, which exhibited superior performance for CCA induced by photothermal effect. Recently, Huang group [13] developed Bi-based MOFs to drive the reaction, they proposed light not only could activate

* Corresponding authors.

E-mail addresses: yuxuefang2008@gmail.com (X.-F. Yu), yangxl@qdu.edu.cn (X. Yang).

¹ <https://orcid.org/0000-0001-6317-724X>

CO₂ indirectly, but also photogenerated holes act as Lewis acid to promote the rate-determined step.

Essentially, the Lewis acid sites prefer to adsorb and polarize epoxides. It is considered to be the rate-limiting ring-opening step, ensuring the reaction is thermodynamically feasible [14]. In terms of dynamics, appropriate heat is necessary due to its endothermic nature no matter such energy is supplied by photothermal or external heating forms. Over the past decade, the Zinc-based Lewis acid has attracted extensive attention for CCA. Huang group [10] found Zn in modified UiO-bpydc MOFs could activate propylene oxide (PO) and promotes LMCT (ligand metal charge transfer) process, thus playing role of synergistic effect of Lewis acid and charge separation. Zhi et al. [15] fabricated Zn-N/carbon and found Zn atoms and N atoms acts as Lewis acid and Lewis base synergistically to drive CCA photothermally. Various Zn-based photothermal catalysts have been developed like ZnS/N doped C [16], N-doped Carbon/ZnO [17], Zn-N-C nanoreactor [18] and others. While it is worth noting that all the Zn-based semiconductor listed above is broad-bandgap responded semiconductor, photons are not adsorbed by Zn-based semiconductor, but are adsorbed by carbon supports and converted to heat. Its essence is thermocatalysis, photon did not take part in catalytic reaction essentially.

As an excellent narrow-bandgap semiconductor, ZnIn₂S₄ attracts extensive research interests owing to adjustable bandgap [19], superior redox capability and robust stability, which is widely employed in PHE (Photocatalytic Hydrogen Evolution), organic synthesis, N₂ fixation and CO₂ reduction reaction etc. [20–22]. Previously Xie and co-workers [23] found one-unit-cell ZnIn₂S₄ layers with V_{Zn} showed superior CO₂ to CO formation rate compared with its counterpart due to higher charge density and efficient carrier separation efficiency. Shi et al. [24] found V_{Zn} vacancy promote reduction of CO₂ to CO₂^{•−} in V_{Zn}-vacancy riched 3D

hierarchical ZnIn₂S₄ because of decreased carrier transport activation energy (Thermal potential of CO₂ to CO₂^{•−} was −1.9 V versus normal hydrogen electrode (NHE) at pH 7). Furthermore, our group either reported plasma synergies with ZnIn₂S₄ to exhibit superior catalytic activity for selective oxidation of aromatic alcohols driven by blue LED [25].

Excitingly, considering the Lewis acid of ZnIn₂S₄ and the excellent visible light absorption capability, ZnIn₂S₄ would be a powerful thermal-photo dual-driven catalyst for CCA reaction compared with other conventional sole thermal driven or thermal_{photo} driven Zn-based catalysts. However, regrettably it has rarely been reported so far. Hence, herein this work synthesized various ZnIn₂S₄ semiconductor photocatalysts with different surface Zinc exposed sites with facile one-pot solvothermal methods, which were evaluated by CO₂ cycloaddition reaction with the assistance of blue LED ($\lambda_{\text{blue light}} = \sim 450$ nm). Various physical-chemical techniques including XRD (X-Ray diffraction), FESEM (field emission scanning electron microscopy), HRTEM (high-resolution transmission electron microscope), XPS (X-Ray photoelectron spectroscopy), NH₃-TPD (NH₃-temperature programmed desorption) and CO₂-TPD (CO₂-temperature programmed desorption) etc have been utilized to investigate structure-activity relationship. In combination with trapping experiments, in situ-EPR (in situ-electron paramagnetic resonance) and DFT (density functional theory) results possible reaction mechanism driven by dual energy type was proposed. In addition, targeting at industrial application, reaction parameters (T, P, t, substrates, etc) as well as recycle robustness were evaluated either.

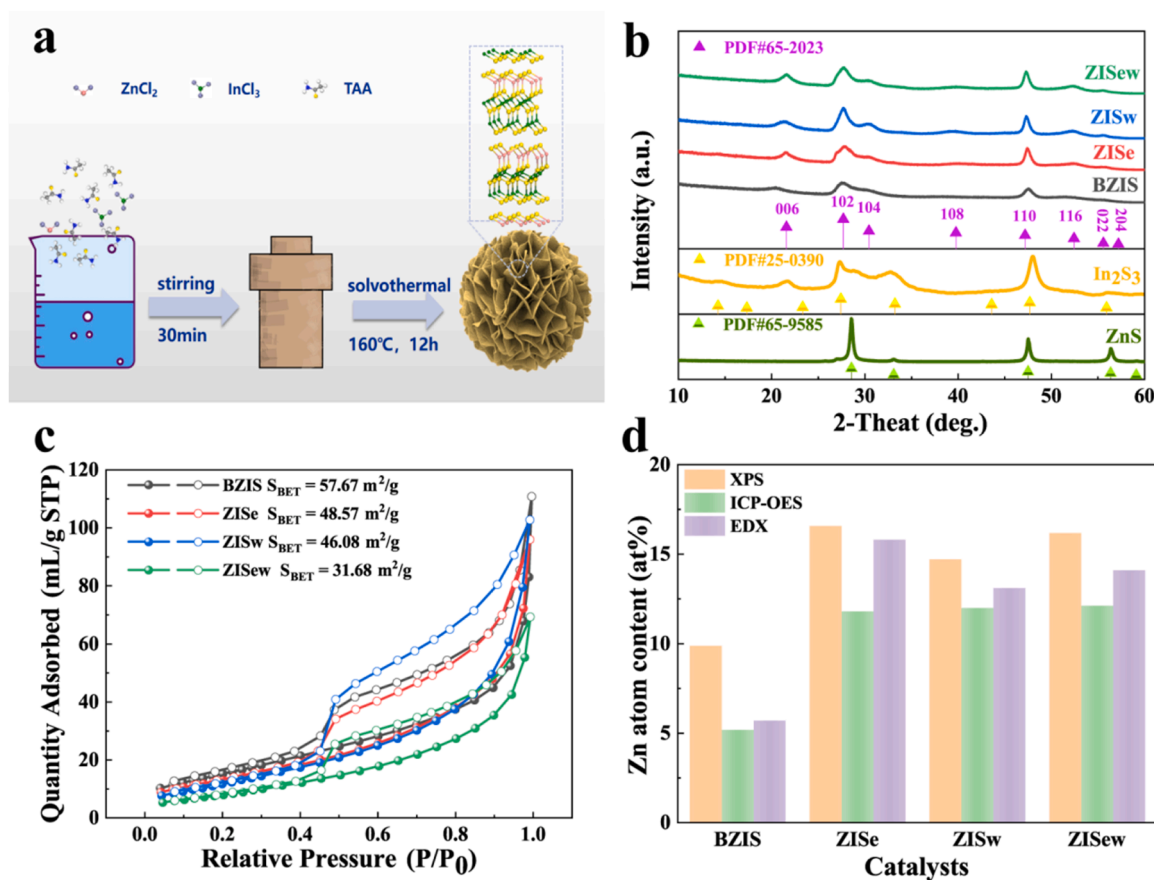


Fig. 1. (a) Synthesized route of ZISe photocatalyst; (b) XRD; (c) N₂-adsorption-desorption isotherm; (d) surface and bulk Zn atomic content determined by XPS, ICP-OES and EDX, respectively.

2. Experimental section

2.1. Synthesizing method of ZISE

ZISE was fabricated by solvothermal method as shown in Fig. 1a. Briefly, ZnCl_2 (1 mmol), $\text{InCl}_3 \cdot 4\text{H}_2\text{O}$ (2 mmol) and TAA (Thioacetamide, 8 mmol) were dispersed into 30 mL ethanol in sequence under continuous stirring for 0.5 h, which was transferred to 100 mL Teflon-lined steel autoclave and maintained at 160 °C for 12 h. Obtained solid products were separated by high-speed centrifuge after the autoclave cooled down to room temperature. The products were further washed and dried, marking as ZISE. Similarly, ZISw and ZISew were synthesized by hydrothermal and mixed solvothermal ($V_{\text{water}}:V_{\text{ethanol}}=1:1$), respectively. BZIS were prepared at 80 °C for 2 h, See [Supplementary information](#) for detailed steps.

2.2. Characterization technique

The XRD were conducted on Smart Lab 3KW (Rigakum, Japan) with Cu K α radiation ($\lambda = 0.15418$ nm). The XPS were obtained from EACALAB Xi+ (Thermo Fisher, USA) with a monochromatic X-ray Al K α ($h\nu = 1486.6$ eV) source calibrated with C 1 s peak at 284.8 eV. The N_2 adsorption-desorption isothermal curve were conducted on 3 H-2000PMC (BeiShiDe, China) at liquid nitrogen temperature. The data analysis method employed BJH (Barrett-Joyner-Halenda) method. The metal content in ZnIn_2S_4 were measured by ICP-OES (Agilent, USA). The micro-morphology were observed and analysis on FESEM by Regulus8100 (Hitachi, Japan). TEM and HRTEM were obtained on JEM 2100 F (JEOL, Japan) operating at 300 kV. The UV-Vis DRS (UV-Vis diffuse reflectance spectra) were measured on a Jena SPECORD 210 PLUS spectrophotometer with integrating sphere and BaSO_4 reflection standard reference. PL spectra were conducted on Edinburgh FLS1000 under 365 nm excitation at room temperature. The CO_2 -TPD, NH_3 -TPD tests were analyzed by BELCAT-A gas adsorption analyzer at 298 K. CO_2 adsorption isotherms were obtained by a Micromeritics analyzer (ASAP 2020) at 298 K. Photoelectrochemical experiments were carried on electrochemical workstation (ChenHua, China) using standard three-electrode system. Electrochemical impedance spectroscopy (EIS) was also obtained in the three-electrode system. In situ-ESR spectra were recorded with Bruker model A300 spectrometer with 300 W Xe lamp.

2.3. Photo-thermal_{Joule}-catalytic CO_2 fixation for the synthesis of cyclic carbonate

The CCA reaction was carried out in 50 mL customized stainless-steel reactor with pressure resistant quartz plate on top. Typically, 35.7 mmol Propylene oxide (PO), 0.3 mmol Tetra-n-butylammonium bromide (TBAB) cocatalyst and 30 mg photocatalysts were added to the reactor in sequence and sealed, which was purged with CO_2 to remove residual air and keep inner pressure to be 1.0 MPa. The reaction was conducted at 80 °C for 8 h under continuous magnetic stirring. The photocatalytic cycloaddition reaction was driven by blue LED (100 mW/cm², its wavelength centered at ~446 nm, See Fig. S20). The reactor was naturally cooled and depressurized, the suspension mixture was centrifuged, the resulted catalyst was reused after washing and drying. The product was diluted with MeCN (acetonitrile) and quantified by GC-FID (HP-5) (Biphenyl as internal standard). The detailed information was recorded in ESI S2.

The yield of product and reaction rate for product were calculated as follows:

$$\text{Yield (\%)} = (n_{\text{PC}}/n_{\text{PO}}) \times 100\% \quad (1)$$

$$\text{Reaction rate (mmol g}^{-1} \text{ h}^{-1}) = n_{\text{PC}} / m_{\text{cat}} / t \quad (2)$$

Propylene carbonate (PC) is the product of the CCA reaction.

n_{PC} : molar amount of PC generated;

n_{PO} : molar amount of initially added PO;

m_{cat} : mass of the catalyst;

t : reaction time.

3. Results and discussion

3.1. Characterization of various samples

Diffraction peaks located at 21.5°, 28.3°, and 47.2° were assigned to characteristic hexagonal ZnIn_2S_4 (PDF#65-2023) [26], no other second phase or impurities phase were observed (Fig. 1b). There aren't diffraction signals can be attributed to binary sulfide ZnS or In_2S_3 , indicating the pure phase structure of hexagonal ZnIn_2S_4 . As shown in Fig. 1c, BET surface areas obtained from BJH calculation method were determined to be 57.67, 48.57, 46.08 and 31.68 m²/g for BZIS, ZISE, ZISw and ZISew, respectively. They all exhibit type IV sorption isotherm with H3 hysteresis loop, indicating mesoporous characteristics [27]. Corresponding pore size distribution (Fig. S1) also testified the mean pore size is mesoporous type. In addition, metal cation in semiconductors could play Lewis acid role in CCA reaction. Hence, bulk and surface element content of catalyst were investigated dialectically by ICP-OES (inductively coupled plasma optical emission spectrometer), EDX (energy dispersive X-Ray spectroscopy) and XPS, respectively, to some extent the former measures the bulk content, while the latter two measures the surface content. As shown in Fig. 1d, Table S1, S2 and S3, ZISE (13.5 wt%), ZISw (13.5 wt%) and ZISew (14.1 wt%) possess much higher Zn content compared with BZIS (6.1 wt%) in bulk materials. Surprisingly, ZISE possess the highest superficial Zn content (16.6 at% XPS; 15.8 at% EDX) compared with ZISw (14.7 at% XPS; 13.1 at% EDX), ZISew (16.2 at% XPS; 14.8 at% EDX) and BZIS (9.9 at% XPS; 5.7 at% EDX), which may have a positive effect on ring-open step of PO (considered as rate-determining step) [12].

BZIS, ZISw and ZISew all exhibits the characteristic marigold-like microsphere (4 ~ 6 μm), which are assembled by interlaced 2D nanosheets (Fig. S2). while the ordered degree of ZISE flower balls assembled by nanosheets is relatively low as shown in Figs. 2a, 2b. Furthermore, TEM also confirms the 3D marigold-like microsphere assembled by ultrathin ZISE nanosheets (Figs. 2c, 2d). The HRTEM (Figs. 2e, 2f and 2g) further demonstrated $d_{(102)} = 0.32$ nm for hexagonal ZnIn_2S_4 [28]. The distorted lattice fringe implied the presence of defects in ZISE photo-catalyst (Fig. 2f).

The elemental compositions as well as surface chemical environment of samples were explored by XPS. Survey spectra confirms Zn, In and S elements in corresponding samples while no other impurities were observed (Fig. 3a). As presented in Fig. 3b, the peaks of Zn 2p centered at 1045.3 eV ($2p_{1/2}$) and 1022.2 eV ($2p_{3/2}$) are assigned to Zn^{2+} [29]. ZISw as well as pristine ZIS remains the same as that of the former. Binding energy signals of In 3d located at 452.5 eV ($3d_{3/2}$) and 444.9 eV ($3d_{5/2}$), belonging to In^{3+} (Fig. 3c) [30]. The peaks of S 2p centered at 162.7 eV ($2p_{1/2}$) and 161.5 eV ($2p_{3/2}$) in Fig. 3d are attributed to S^{2-} [31]. Additionally, the binding energy of Zn^{2+} , In^{3+} and S^{2-} in ZISew tend to move to high BE (Binding energy) direction, which probably hint the presence of S defects. The binding energy of S 2p, Zn $2p_{1/2}$, Zn $2p_{3/2}$ belonging to ZnS is 168.3 eV, 1045.7 eV and 1022.8 eV. BE value of S 2p, In $2p_{3/2}$, In $2p_{5/2}$ belonging to In_2S_3 is 162.9, 161.7 eV, 452.2 eV and 444.7 eV, respectively. In addition, the binding energy of ZISE is very different from that of single ZnS and In_2S_3 materials, which proves that the surface species of ZnIn_2S_4 are the same as the bulk phase, and there are no unreacted ZnS and In_2S_3 microcrystals (Fig. S3).

Optical adsorption property is investigated by UV-Vis-DRS. As presented in Fig. 4a, In_2S_3 exhibits superior visible light adsorption efficiency and its adsorption edge extends to ~650 nm, conversely ZnS is a typical UV-response semiconductors and its maximum adsorption wavelength does not exceed ~400 nm [32]. ZISw, ZISEw as well as BZIS have a similar optical property, the maximum adsorption wavelength mainly centered at ~496 nm. Interestingly, the adsorption edge of ZISE

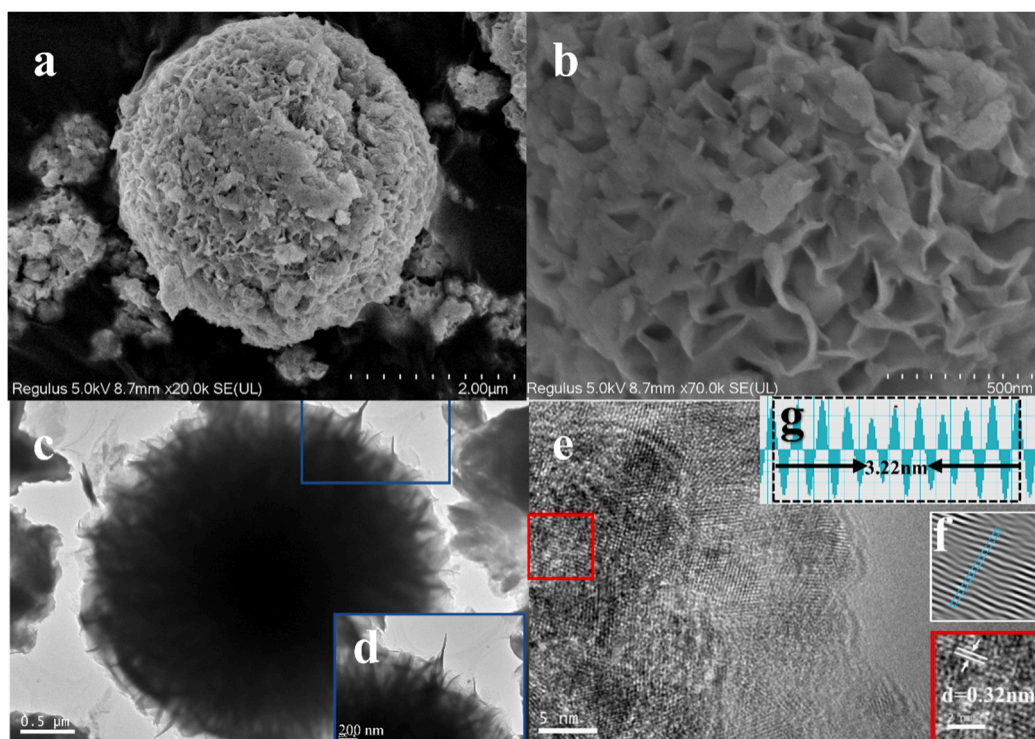


Fig. 2. FESEM of (a, b) ZISe; (c, d) TEM and (e, f, g) HRTEM of ZISe.

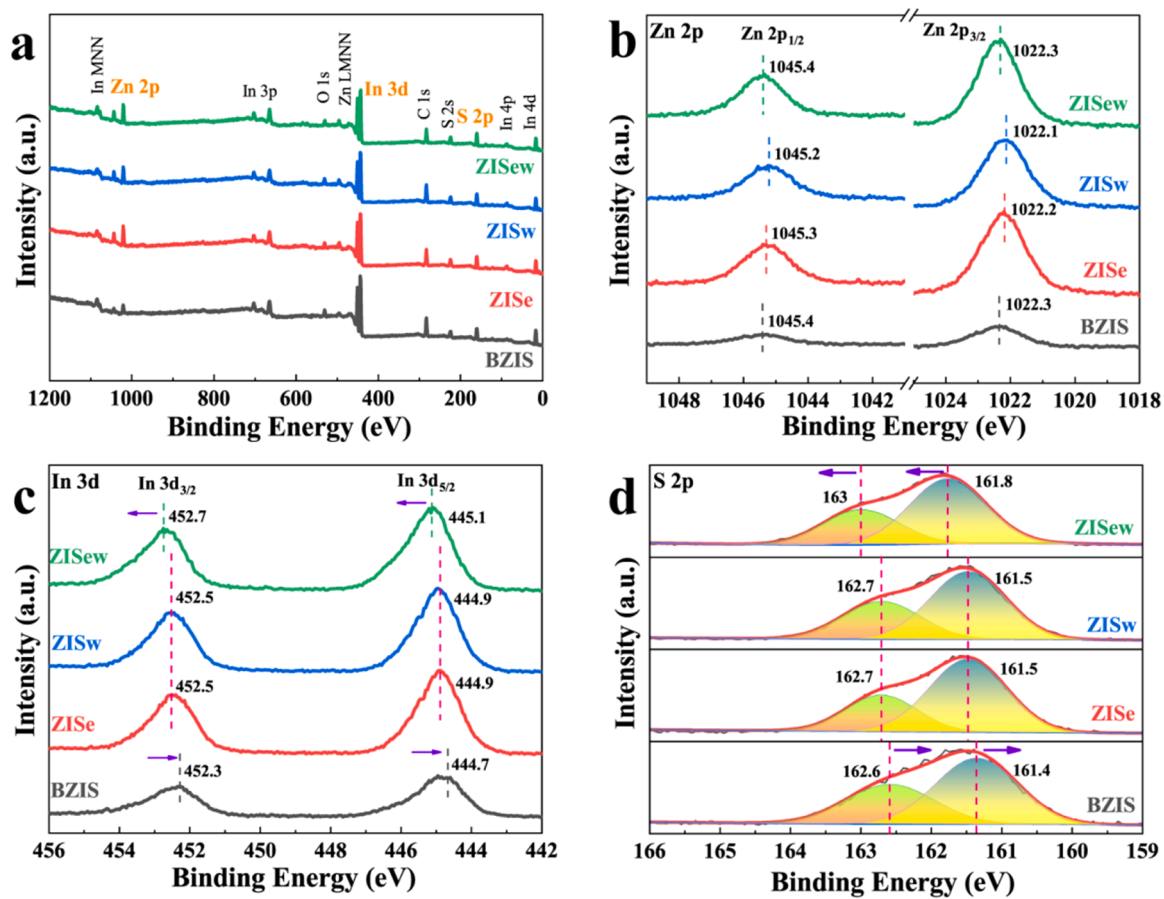


Fig. 3. (a) XPS survey; (b-d) Zn 2p, In 3d, S 2p of photocatalysts.

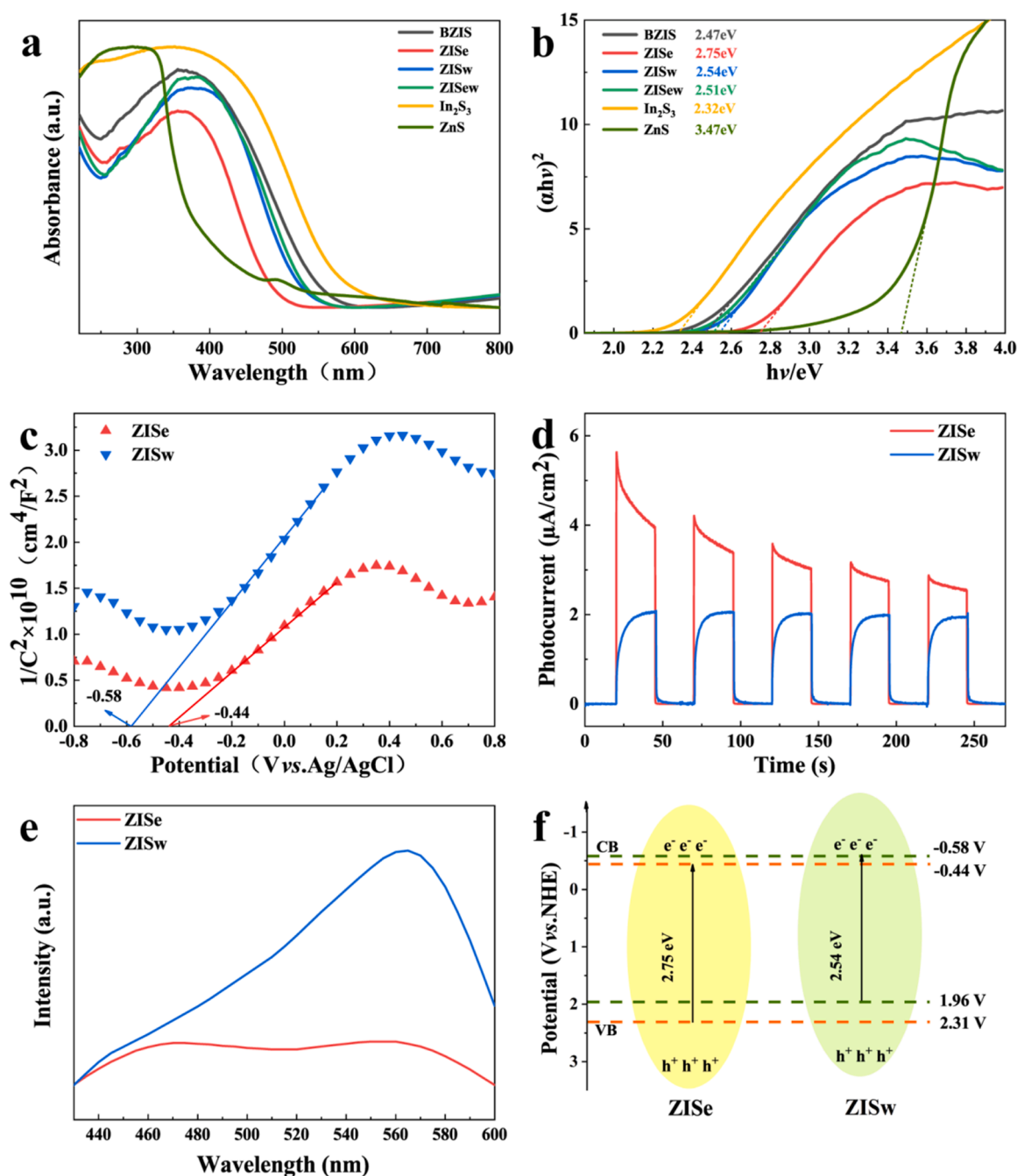


Fig. 4. (a) UV-Vis-DRS; (b) Tauc plots; (c) Mott-Schottky plots; (d) Transient photocurrent responses; (e) Steady PL spectra; (f) Schematic illustration of band structure for ZISe and ZISw.

tends to move to UV region compared with its counterpart discussed above, which implying the photon adsorption efficiency cannot determine the catalytic activity we discussed later. Additionally, E_g of samples was calculated by Kubelka-Munk transformation [33]. Corresponding E_g values was estimated to be 2.47, 2.75, 2.54, 2.51, 2.32 and 3.47 eV for BZIS, ZISe, ZISw, ZISew, In_2S_3 and ZnS, respectively (Fig. 4b). Mott-Schottky (M-S) curves were conducted to determine band structure. Positive slope of ZIS confirms its n-type semiconductor (Fig. 4c) [34]. The FBP (flatband potential) of ZISe and ZISw are -0.44 V and -0.58 V vs. Ag/AgCl, respectively, implying strong reduction potentials. For details of the calculation of the band structure, refer to S3. The N_d (carriers' density) was calculated by the following equation [35]:

$$N_d = 2 / (e \epsilon \epsilon_0) \left[\frac{d(1/C^2)}{dV} \right]^{-1}$$

where e , ϵ and ϵ_0 are the electron charge (-1.602×10^{-19}), dielectric constant (about 4.73 for ZnIn_2S_4) [36] and vacuum permittivity (8.854×10^{-12}), respectively. The slope of ZISe (2.44×10^{10}) is smaller compared to that of ZISw (3.54×10^{10}), demonstrating its higher carrier density. Exactly, ZISe exhibits a higher N_d (1.34×10^{19}) than that of ZISw (8.5×10^{18}) (1.58 times larger), suggesting more carrier transport in ZISe. As listed on Fig. 4f, the ZISe possess much stronger oxidize ability compared with ZISw due to its more positive of VB potentials.

The separation efficiency and recombination degree of photoinduced carriers in photocatalyst always determines the carriers' utilization

efficiency [37]. As shown in Fig. 4d, transient photocurrent response demonstrates the photocurrent intensity of ZISe is much larger than that of ZISw (1.7 times), which confirming the better ability of the former to separate photogenerated carriers [38]. In addition, the electrochemical impedance spectroscopy (EIS) Nyquist plots have been collected to further examine the carrier's separation. As shown in Fig. S4, it is obvious the semicircle radius of ZISe is much smaller than that of ZISw, which indicates the former has a lower charge-transfer resistance, resulting in more efficient charge separation [39].

Photoluminescence (PL) is a strong tool to characterize carriers' separation efficiency. Generally speaking, the higher the PL intensity, the stronger the recombination degree [40]. As demonstrated in Fig. 4e, the center emission wavelength of ZISw located at ~ 565 nm, which is in accordance with previous literature [34]. It is found that the ZISe possess rather weak peak intensity compared with its counterpart ZISw, which implying its much higher of carriers' utilization efficiency and rather low degree of recombination either [41].

TGA was preformed to evaluate thermal stability of the ZnIn_2S_4 (Fig. S5) [42]. 1% mass loss were ascribed to physical adsorption H_2O (~ 200 °C), mass loss does not exceed 3% until the temperature increase to 500 °C. Therefore, the excellent thermal stability of ZISe guarantees the reliability of following TPD experiments results. Significantly, Lewis acidity and basicity play key role in CCA reaction according to previous literatures [43,44]. Therefore, NH_3 -TPD and CO_2 -TPD of catalysts were conducted. Generally speaking, the desorption peaks below 200 °C and above 200 °C are attributed to weak acid sites and strong acid sites respectively [45]. As shown in Fig. 5a and Table S4, ZISe show higher number of acidic sites compared to ZISw, specifically, weak acidic sites and strong acidic sites appears at 115.1 °C with NH_3 adsorption capacity of 0.035 mmol/g and 270.2 °C with 0.207 mmol/g, respectively. However, ZISw possess relatively less acidic sites number and intensity, the

total NH_3 adsorption capacity is estimated to be 0.143 mmol/g, which is only about 59% of ZISe catalyst. Furthermore, Lewis acid sites were confirmed by Pyridine-adsorbed FTIR as shown in Fig. S6, it can be observed absorption bands appears at around 1584 cm^{-1} and 1441 cm^{-1} , which represent the adsorption peaks of Lewis acid sites on ZISe, the bands at 1482 cm^{-1} represents adsorption signal of L+B [46].

Meanwhile, CO_2 adsorption ability of catalysts have a great impact on CCA reaction [47]. CO_2 physical-adsorption isotherm were investigated as shown in Fig. 5b. CO_2 physisorption amount of ZISe achieves $5.2737\text{ cm}^3/\text{g STP}$, which was much larger than that of the ZISw ($1.9931\text{ cm}^3/\text{g STP}$). Noteworthy the S_{BET} is almost the same for both catalysts as shown in Fig. 1c (ZISe: $48.57\text{ m}^2/\text{g}$; ZISw: $46.08\text{ m}^2/\text{g}$), thus the strong affinity of CO_2 is ascribed to surface Lewis basic sites for ZISe. In addition, unclosed loop suggests CO_2 chemisorption to a large extent [48]. Much enhanced CO_2 affinity would further promote CO_2 activation over surface of catalyst. Deeply, CO_2 chemisorption behavior were investigated by the CO_2 -TPD technique [44]. As depicted in Fig. 5c and Table S5, ZISw exhibits a broad peak with low intensity at a slightly lower temperature of 251.2 °C, and its total CO_2 adsorption capacity (0.021 mmol/g) is only 10.4% of that of the ZISe catalyst. The weak and strong Lewis basic sites appear at 120 and 267.3 °C for ZISe, respectively. The former peak might be attributed to CO_2 physisorbed and the latter could be assigned to the strong chemisorption of CO_2 on S^{2-} Lewis basic sites. The total CO_2 adsorption capacity achieves 0.20 mmol/g, which is almost 9.6 times larger than that of the ZISw (Fig. 5d). Noticeably, CO_2 desorbed at higher temperature for ZISe with strong desorption peak intensity compared to ZISw, suggesting strong Lewis acid-base interactions on ZISe, thus facilitating capture of CO_2 molecules powerfully. In ZnIn_2S_4 catalytic system, S^{2-} in the crystal structure is expected to be responsible for CO_2 chemisorption. Abundant amount of Lewis basic site of ZISe catalyst is conducive for the chemisorption and

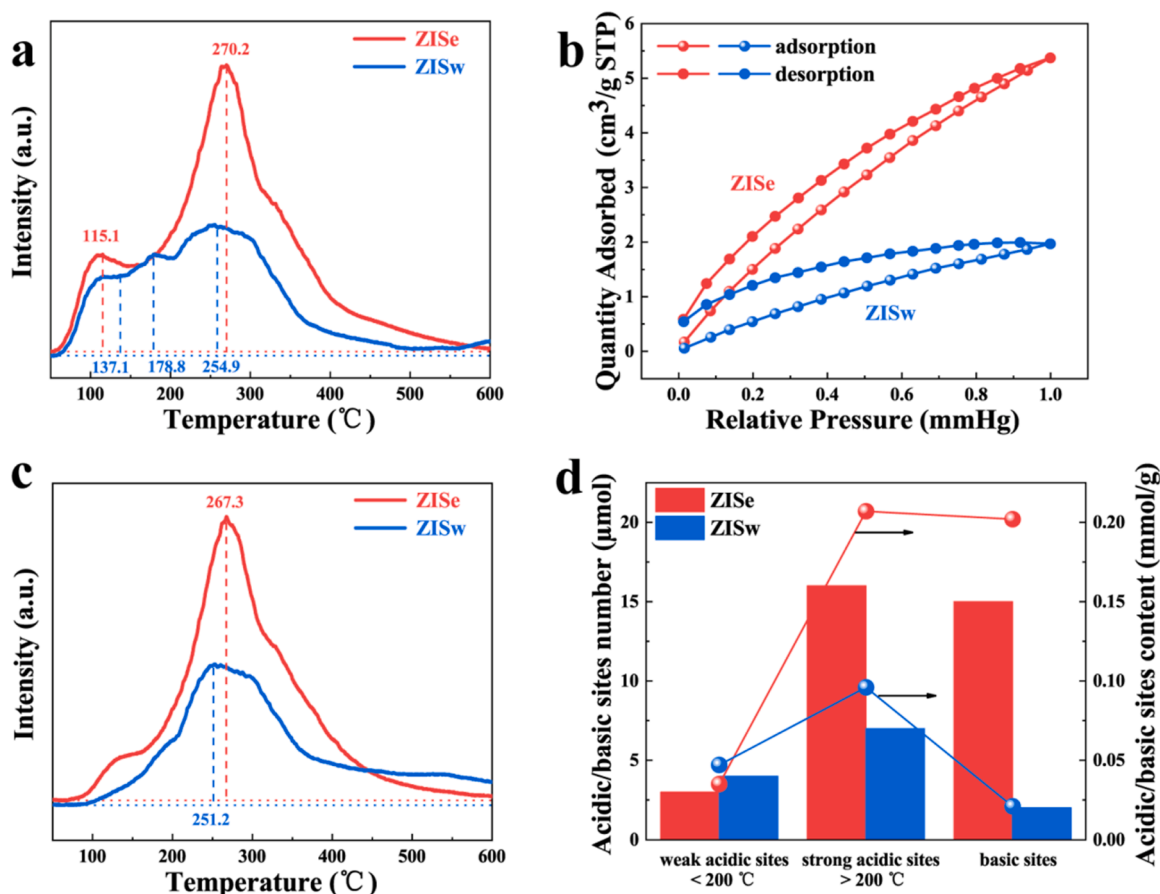


Fig. 5. (a) NH_3 -TPD; (b) CO_2 physical-adsorption isotherm; (c) CO_2 -TPD; (d) Number of acidic sites and basic sites for ZISe and ZISw.

activation of inert CO_2 molecule. Therefore, a large number of superficial Zn^{2+} Lewis acidic sites for open-ring rate-determining step cooperates with S^{2-} Lewis basic sites for CO_2 adsorption/activation synergistically promote the CCA reaction rate. It was concluded that efficient CO_2 adsorption and activation was realized for ZISE because of improved CO_2 physical and chemisorption, potentially contributing to CO_2 photoreaction [49].

3.2. CCA catalytic performance

The thermal-photocatalytic performance for CCA reaction over various catalysts were evaluated under certain conditions. As shown in

Fig. 6a (Table 1, Entry 1, 2), (No catalyst)/TBAB system exhibits 21.01% and 29.52% of conversion for PO under dark and illumination conditions, respectively. Surprisingly, almost all binary metal sulfides and ternary metal sulfides promote the CCA reaction. To be specific, as high as 92.3% of conversion can be achieved within 8 h under blue LED illumination over ZISE catalysts, which is 4.40 times larger than pristine (No catalyst) /TBAB/dark system. Either, it is 2.13, 1.54 and 1.51 times higher than that of BZIS, ZISw and ZISew, respectively (Table 1, Entry 3, 8, 10, 12). In addition, thermodynamic calculation were carried out to explore the reaction. As shown in Fig. S7, ΔG^0 decreased from -9.768 to -12.078 kJ/mol with the temperature increase from 353 to 393 K, and remaining negative all the time. It indicated CO_2 cycloaddition

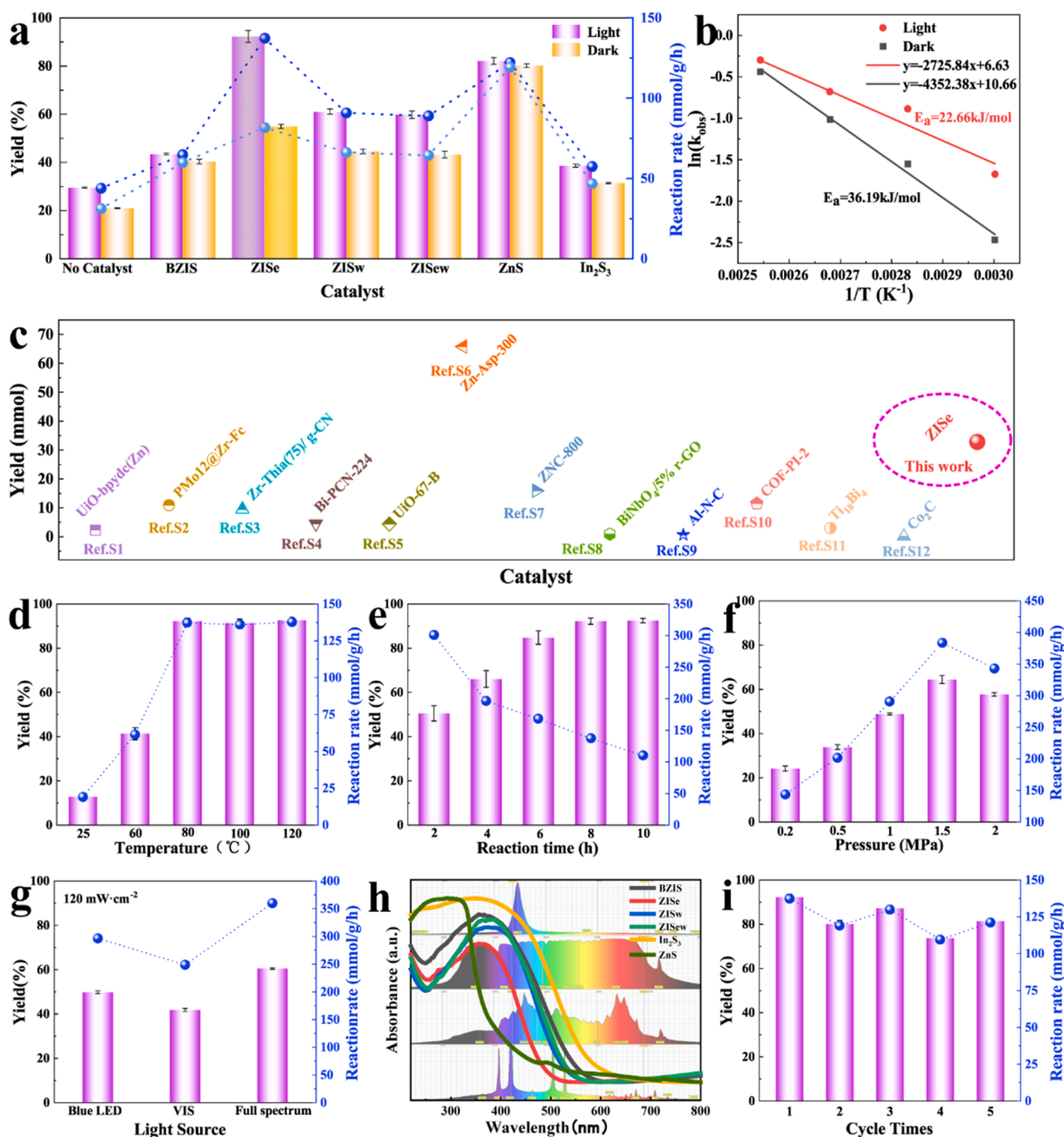
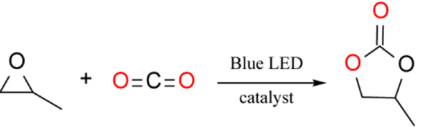


Fig. 6. (a) Yield of different catalysts for CO_2 cycloaddition. (b) Calculated apparent activation energy E_a for ZISE under dark and light irradiation. (c) Catalytic performance of reported catalysts for CCA reaction and ZISE catalyst. (d) reaction temperature. (e) reaction time. (f) reaction pressure. (g) light source ($120 \text{ mW}\cdot\text{cm}^{-2}$, 2h). (h) UV-Vis-DRS and the spectrum of light source. (i) Cyclability of ZISE.

Table 1
CO₂ Cycloaddition performance for different catalyst^[a].



| Entry | Blue LED | Tem (°C) | Catalyst | Cocatalyst | Yield (%) ^[b] |
|-------|----------|----------|---------------------------------|------------|--------------------------|
| 1 | + | 80 | None | TBAB | 29.52 |
| 2 | - | 80 | None | TBAB | 21.01 |
| 3 | + | 80 | ZlSe | TBAB | 92.26 |
| 4 | - | 80 | ZlSe | TBAB | 54.98 |
| 5 | + | 25 | ZlSe | TBAB | 12.85 |
| 6 | - | 25 | ZlSe | TBAB | 7.50 |
| 7 | + | 80 | ZlSe | - | 0.88 |
| 8 | + | 80 | BZIS | TBAB | 43.24 |
| 9 | - | 80 | BZIS | TBAB | 40.33 |
| 10 | + | 80 | ZISw | TBAB | 59.78 |
| 11 | - | 80 | ZISw | TBAB | 44.55 |
| 12 | + | 80 | ZISew | TBAB | 61.05 |
| 13 | - | 80 | ZISew | TBAB | 43.26 |
| 14 | + | 80 | ZnS | TBAB | 82.15 |
| 15 | - | 80 | ZnS | TBAB | 80.16 |
| 16 | + | 80 | In ₂ S ₃ | TBAB | 38.65 |
| 17 | - | 80 | In ₂ S ₃ | TBAB | 31.44 |
| 18 | + | 80 | g-C ₃ N ₄ | TBAB | 23.45 |
| 19 | + | 80 | ZIF-8 | TBAB | 43.63 |
| 20 | + | 80 | UIO-66 | TBAB | 42.75 |
| 21 | + | 80 | Zr-β molecular sieve | TBAB | 48.49 |
| 22 | + | 80 | Al-Zn hydrotalcite | TBAB | 69.50 |

[a] 30 mg catalyst, co-catalyst TBAB (0.3 mmol), PO (35.7 mmol), 1 MPa, 8 h;

[b] PC was quantified by GC-FID with biphenyl as internal standard.

reaction on ZlSe was a spontaneous endothermic disorder reaction within the temperature range (353–393 K). And the degree of spontaneous reaction became greater with the increase of reaction temperature.

For comparison, binary metal sulfides ZnS and In₂S₃ were also employed as catalysts for reaction (Table 1, Entry 14–17). As shown in Fig. 6a, ZnS showed relatively high conversion of 82.2%, while it cannot be further promoted by blue light excitation owing to its inherent UV responded character. Liu et al. proposed ZnS/N-doped carbon exhibited superior CO₂ cycloaddition performance [50]. The mechanism of ZnS driven CCA reaction is similar to that of ZnO. That is, it plays role of Lewis acid, Zn²⁺ could coordinate and polarize O atom in PO molecules. Then Br⁻ nucleophilic attack less sterically hindered β-carbon atom of epoxide to complete open-ring step of PO (The rate-determined step of CCA reaction) [51]. The In₂S₃ showed the worst catalytic activity among all the catalytic system. Interestingly, although catalytic performance of ZlSe is apparently inferior than that of the ZnS in dark, the activity was boosted sharply by blue light excitation and eventually exceeds the activity of ZnS. In order to clarify such improvement is ascribed to photocatalysis or thermal_{photo} (Photoinduced thermal) catalysis, control experiments were conducted. The above point is important because the former is photocatalysis while the latter is thermalcatalysis essentially. Firstly, the thermal_{photo} effect of blue LED and other light sources (visible light, full-spectrum light) on catalysts as well as reactor were evaluated by Infrared thermal imaging thermometer and K-type thermocouple wire respectively. As shown in Fig. S8, the temperature of ZIS small disk rise to 26.7 °C from ambient temperature of 16.9 °C, which implies the thermal_{blue LED} effect of blue LED is rather limited. Considering the actual reactor conditions, such increment ΔT 9.8 °C is further largely weakened in actual catalytic reaction system as shown in Fig. S11. The temperature of reactor rise to 59.1 °C from heating temperature of 64.4 °C under blue LED illumination (oil bath temperature set is 80 °C). If we define the external oil heating temperature as thermal_{Joule} and photoinduced thermal as thermal_{photo}, then we can use thermal_{Joule} to

compensate thermal_{photo} in dark condition, that way thermal_{photo} is shielded and the improvement of catalytic activity is solely ascribed to photocatalysis. At the same temperature, the effect of blue light on the reaction is obvious as show in Table. S9, Fig. S12, blue light brings about twice the efficiency of the reaction, which is not caused by thermal_{photo}, but by photocatalysis.

The common Zinc Lewis acid were conducive to the CCA reaction according to the previous literatures, hence some catalysts were also compared with ZIS catalyst under same conditions. As shown in Table 1 (Entry 19–21), specifically ZIF-8, UiO-66 and Zr-β-zeolite showed inferior performance of 43.6%, 42.8% and 48.4% of conversion, respectively. The versatile g-C₃N₄ photocatalyst exhibits an inferior catalytic conversion of 23.5% for PO due to the absence of Lewis acid sites [52] (Table 1, Entry 18). Zn-Al hydrotalcite achieved a yield of 69.5% because of abundant of Lewis acid sites (Table 1, Entry 22). Therefore, ZlSe synthesized in pure ethanol solvent exhibits rather superior catalytic activity for CCA reaction under blue LED illumination compared to reported conventional catalysts. Deeply, the activation energy E_a of ZlSe catalytic system under dark and illumination conditions are calculated by Arrhenius plot as shown in Fig. 6b. Obviously, the E_a under light irradiation (22.7 kJ/mol) is much smaller than that of dark conditions (36.2 kJ/mol), implying different reaction path under light illumination. Furthermore, ZlSe exhibits rather comparable catalytic performance compared with previous work as shown in Fig. 6c and Table 2. the total product Propylene carbonate (PC) achieves 33.0 mmol, which is apparently superior than most reported catalysts. Even better, such thermal_{Joule}-photo-catalytic system is typical solvent-free reaction and achieves lab-scale, rather than micro reaction. Control experiment was also conducted to explore impact of influencing factor on catalytic performance for ZlSe. As shown in Table 1, ZlSe exhibits the high conversion of 54.98% in dark. Without TBAB, ZlSe, ZlSe+blue light, the conversion decreased to 0.88%, 29.52% and 21.01%, respectively, which highlighting synergistic effect of TBAB, photocatalyst and light (Table 1, Entry 1, 2, 4, 7).

3.3. Influence of reaction parameters

The effect of temperature, pressure, reaction time and light source type on PC conversion and yield were investigated in detail. As shown in Fig. 6d (Table 1, Entry 5), ZlSe/TBAB only reaches conversion of 12.85% and reaction rate of 19.11 mmol/g/h at ambient temperature (25 °C). Catalytic activity achieves maxim platform 92.3% at 80 °C. Further elevated temperature would not lead to further improvement of activity. Hence optimal reaction temperature was set to be 80 °C unless otherwise specified.

The conversion rate increased with prolonged reaction time, and the conversion is 92.3% for 8 h (Fig. 6e). The reaction pressure has obvious promoting effect for reaction due to the Le Chatelier equilibrium towards low pressure direction (Fig. 6f). The catalytic performance was improved with increase of pressure. Additionally, light source has significant effect on the catalytic performance as in the following order: Full-spectrum>Blue LED>Vis with same light intensity (120 mw·cm⁻²) at different reaction time (Fig. 6g). On the one hand, blue light matches the wavelength range of absorbed light of ZlSe well as shown in Fig. 6h, although full spectrum apparently boosts the CCA reaction rate while blue LED has the advantages of scalability and easy assembly in practical applications. Thus, it is feasible to use blue light synergistic thermo catalysis to enhance catalytic performance of ZlSe. The recycling performance of catalyst is necessary for practical industrial application. Apparently, 80% conversion after four times of recycle can be kept (Fig. 6i). XRD, SEM and XPS (Fig. S13, S14, S15) were also examined before and after the reaction. Although the surface morphology changes slightly from FESEM images, surface elemental valence remains the same as fresh one, meaning ZlSe catalyst has the potential for sustainable industrial application. Furthermore, excellent yield of cyclic carbonate were achieved with simulated industrial waste gas (CO₂/N₂ ~

Table 2Comparison of CO₂ cycloaddition rate of different catalysts.

| | Catalyst | Dosage | Epoxide | Time | Co-catalyst/ Solvent | Light | T (K) | P (MPa) | Con (%) | Sel (%) | Yield (mmol) | Reaction rate (mmol g ⁻¹ h ⁻¹) | References |
|----|----------------------------------|--------------|-----------------------------------|------|---|---|----------|------------|------------|------------|-----------------|--|------------|
| 1 | ZiSe | 30 mg | PO(35.7 mmol) | 8 h | TBAB/None | Blue LED | 353 | 1 | 92.3 | > 99 | 32.9 | 137.1 | This work |
| 2 | ZiSe | 30 mg | PO(35.7 mmol) | 2 h | TBAB/None | full spectrum | 353 | 1 | 66.9 | > 99 | 23.9 | 398.3 | This work |
| 3 | UiO-bpydc (Zn) | 20 mg | PO | 6 h | TBAB/None | full spectrum | 298 | 0.1 | – | – | 2.3 | 19.2 | [10] |
| 4 | PMo12 @Zr- Fc | 5 mg | SO(12.5 mmol) | 8 h | TBAB/None | Simulated sunlight 0.4 W/ cm ² | 353 | 0.1 | – | – | 10.9 | 363.3 | [53] |
| 5 | Zr-Thia(75)/ g-CN | 50 mg | ECH(10 mmol) | 24 h | DMAP/None | $\lambda > 360$ nm | 298 | 0.1 | 90.8 | 99 | 9.5 | 7.9 | [45] |
| 6 | Bi-PCN-224 | 30 mg | PO(4.5 mmol) | 6 h | TBAB/None | full spectrum | – | 0.1 | 99 | – | 4.5 | 25.0 | [13] |
| 7 | UiO-67-B | 10 mg | PO(5 mL) | 6 h | TBAB/None | full spectrum | 298 | 0.1 | – | – | 4.4 | 73.3 | [48] |
| 8 | Zn-Asp-300 | 100 mg | ECH (71.4 mmol) | 4 h | TBAB/None | 200–1100 nm | – | 0.1 | – | 96.3 | 65.8 | 164.5 | [17] |
| 9 | ZNC-800 | 20 mg | PO (20 mmol) | 10 h | TBAB/None | full spectrum 1000 mW·cm ⁻² | – | 0.1 | – | – | 15.9 | 79.5 | [15] |
| 10 | BiNbO ₄ /5% r-GO | 50 mg | PO(100 μ L) | 24 h | ⁿ Bu ₄ NBr/ acetonitrile, methanol (12 mL) | visible-light | 353 | 1.48 | – | – | 0.93 | 0.8 | [54] |
| 11 | Al-N-C | 20 mg | EBH (0.67 mmol) | 9 h | TBAB/ DMF (2 mL) | full spectrum 400 mW·cm ⁻² | – | 0.1 | 95 | – | 0.64 | 3.6 | [14] |
| 12 | COF-PI-2 | 1.0 mol % | EBH (11.6 mmol) | 24 h | None/None | $\lambda > 400$ nm 80 mW·cm ⁻² | 298 | 0.1 | – | – | 11.5 | – | [55] |
| 13 | Ti ₁₈ Bi ₄ | 20 μ mol | 1,1-hexene epoxide (3 mmol) | 14 h | TBAB/None | full spectrum | 293 | 0.1 | 100 | 100 | 3 | – | [43] |
| 14 | Co ₂ C | 25 mg | ECH (0.15 mmol) | 15 h | TBAB/ MeCN | blue LEDs $\lambda = 450$ nm | – | 0.1 | – | – | 0.14 | 0.4 | [56] |

v15/v85) as feed gas under 1 MPa pressure as well as blue light illumination for 4 h for ECH (Fig. S16).


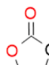

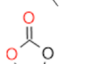
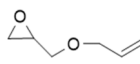
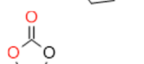
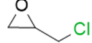
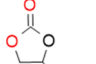
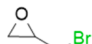
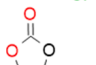
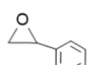
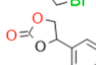
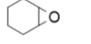
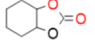
3.4. Substrate scope

Substrate scope for ZiSe catalysts were investigated broadly to explore the potential and general applicability for CCA reaction with various epoxides [57]. As summarized in Table 3, good yield and excellent selectivity were achieved for both PO as well as halogen-substituted PO (Table 3, Entry 1, 4–5). Obviously, big steric hindrance effect would impede ring-open step of epoxide, thus obstruct the nucleophilic attack of TBAB (Table 3, Entry 7) [17]. The product was confirmed by GC-MS (Fig. S17, S18).

3.5. Plausible reaction mechanism

DFT calculation were conducted to deeply investigate the reaction mechanism. Firstly, the adsorption behaviors of PO and CO₂ on the ZnIn₂S₄ (001) surface were examined. To do this, the ZnIn₂S₄ (001) surface was constructed by using the 4 × 4 unit cells containing single layer. Possible adsorption sites S, Zn, In, S-S, S-Zn and S-In bridges in each termination (ZnS or InS) of ZnIn₂S₄ (001) surface, together with the various orientations of adsorbates have been considered. As shown in Fig. 7a, it is found that both CO₂ and PO prefer to adsorb on the ZnS termination of ZnIn₂S₄ (001) surface accompanied by the upward of one In atom in the subsurface. In detail, PO tends to strongly adsorb on the Zn atom of ZnIn₂S₄ (001) surface with the formation of Zn-O, and two C-O bond lengths in PO increase about 0.03 Å, which will be benefit for its subsequent ring opening process. The corresponding adsorption strength is as strong as – 1.33 eV with apparent charge transfer from ZnIn₂S₄ (001) to PO (0.04 e) (Fig. 7c). In contrast, adsorption strength of CO₂ on ZnIn₂S₄ is weaker than PO, and calculated adsorption energy and charge transfer values are only – 0.63 eV mainly on S-sites and 0.001e, respectively.

Table 3CO₂ Cycloaddition with various substrates ^[a].

| Entry | Substrate | Product | Conversion (%) ^[b] |
|------------------|--|---|-------------------------------|
| 1 |  |  | 92.3 |
| 2 ^[c] |  |  | 100 |
| 3 ^[c] |  |  | 98.3 |
| 4 ^[d] |  |  | 95.4 |
| 5 |  |  | 99.5 |
| 6 ^[d] |  |  | 93.7 |
| 7 ^[c] |  |  | 29.4 |

[a] 30 mg catalyst, co-catalyst TBAB (0.3 mmol), PO (35.7 mmol), 1 MPa, 8 h, blue led light;

[b] The epoxide was quantified by GC-FID with biphenyl as internal standard;

[c] 30 mg catalyst, TBAB (0.3 mmol), epoxide (10 mmol), 1 MPa, 8 h, blue led light;

[d] 30 mg catalyst, TBAB (0.3 mmol), epoxide (12 mmol), 1 MPa, 8 h, blue led light.

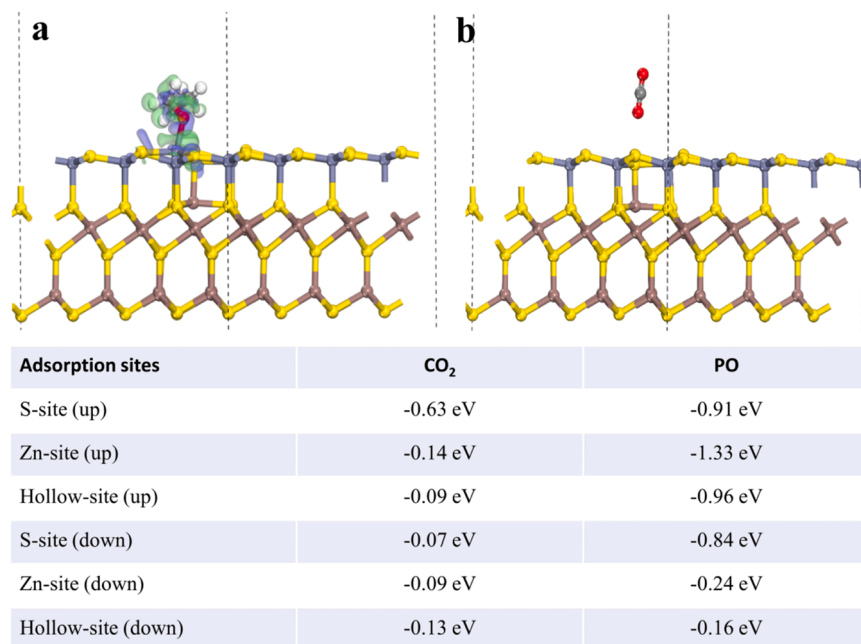


Fig. 7. Structures and charge density differences (CDD) for adsorptions of (a) PO and (b) CO₂ on ZnS termination of ZnIn₂S₄ (001) surface, respectively. green and blue colors represent the electron rich and deficient regions, respectively. (c) The adsorption energies of CO₂ and PO on various sites of ZnIn₂S₄ (001) surface based on DFT calculations.

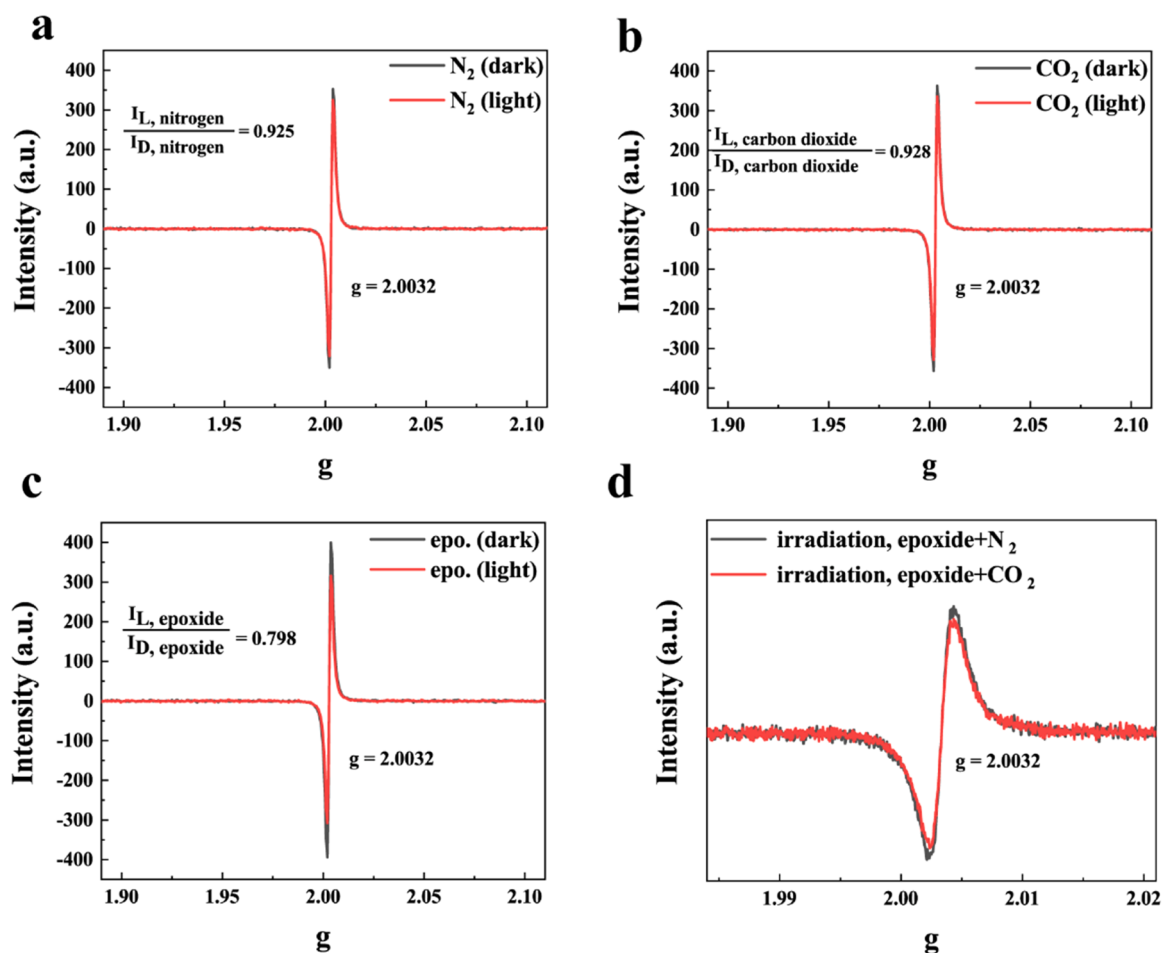


Fig. 8. In-situ ESR spectra of ZISE under different conditions: (a) N₂ atmosphere; (b) CO₂ atmosphere, and (c) added PO in N₂ atmosphere; (d) PO+N₂, PO+CO₂.

CDD were calculated to investigate adsorption behaviors of PO and CO₂ on ZnIn₂S₄ (001) shown in Fig. 7a, 7b. Apparent charge transfer between ZnIn₂S₄ and PO is observed, which is consistent with above discussion. Particularly, both e-rich and e-deficient could be found between Zn and PO, which is mainly due to the coexistence of the electron transfers from PO to the *d* orbital of Zn and from the Zn to the *p* orbital of PO. Such “back donation” effect could effectively weaken the stability of PO, which will trigger the subsequent catalytic processes. In addition, S adjoined near Zn-PO adsorption site tend to take part in charge transfer process, implying either presence of interaction of S with PO. While in the case of CO₂, almost no charge transfer could be found in CDD analysis. To sum up, both strong interaction strength as well as electronic coupling between PO and ZnIn₂S₄ (001) surface would promote charge separation and diffusion during photocatalytic reactions.

The electron flow direction of reaction system under illumination could be reflected by peak intensity of in situ-ESR. *g* factor of 2.0032 can be assigned to the unpaired electron in ZISE. The signals of unpaired electron of ZISE can be observed in dark conditions, which implies the presence of defect in ZISE. As shown in Fig. 8a the intensity ratio of $I_{L,nitrogen}/I_{D,nitrogen}$ was calculated to be 0.925, while the value of $I_{L,CO_2}/I_{D,CO_2}$ was equals to be 0.928 (Fig. 8b), therefore suggesting the photo-generated electron of ZISE cannot be transferred to CO₂ molecules (In consideration of large CB electron potential of CO₂→CO₂•⁻ (−1.9 V vs NHE). It is consistent with the Al-N-C in previous report[14]. Similarly, the photoinduced electron tend to transfer to adsorbed PO since the $I_{L,epoxide}/I_{D,epoxide}$ was calculated to be 0.798 (Fig. 8c). Furthermore, the value of $I_{L,epoxide+CO_2}$ decreases a little compared with that of $I_{L,epoxide+N_2}$ ($I_{L,epoxide+N_2}/I_{L,epoxide+CO_2}=1.13$, Fig. 8d), further testifying the trends that photoinduced electron may transferred to CO₂ indirectly with PO as electron bridge.

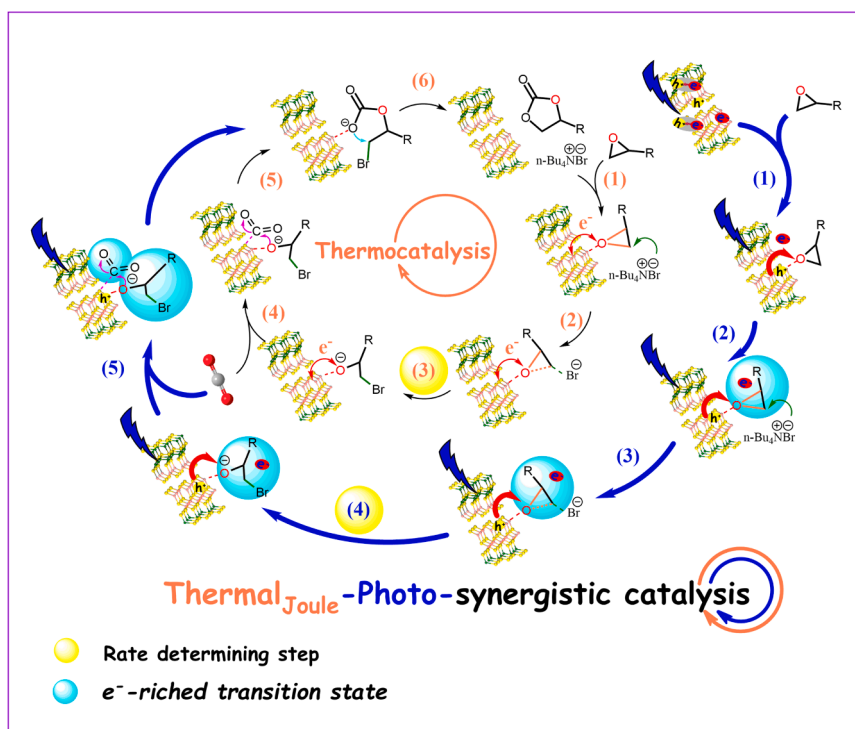
Correspondingly, electron and hole scavenger's experiments have been conducted further. Methanol, 1,4-pBQ and AgNO₃ were employed as hole quencher and electron quencher, respectively. As shown in Fig. S21, yield decreases profoundly with methanol scavenger (from 92.3% to 53.9%), this may be due to methanol quenching and sacrificing the photogenerated holes, which is usually considered as the

photogenerated Lewis acid site. 1,4-pBQ quenched photoinduced electrons and impeded the electron transfer path from ZISE to CO₂ (from 92.3% to 75.4%), it should be noted that such range of decline is obviously smaller than that of methanol, indicating methanol has a stronger inhibition effect on reaction, which may be because photoinduced holes dominate the open-ring step of PO, being considered as rate-determining step of CCA reaction. Finally, AgNO₃ tremendously hinder the reaction efficiency no matter under illumination (19.9%) or dark conditions (7.7%), the similar phenomenon has also been observed by Wang et al. [43]. Besides the quenching effect of Ag⁺ for electron, it is proposed that the plugging effect of Ag⁺ to S²⁻ may be another important factor, S²⁻ were considered to be one of active site for interaction with PO as well as CO₂ according to DFT results.

Possible thermal_{Joule}-photo_{nonthermal}-synergistic catalytic mechanism is proposed shown in Scheme 1. One hand, reaction goes on with classic thermocatalysis mechanism in absence of light illumination. Lewis acidic site Zn²⁺ in ZISE tend to activate PO, enlarging C-O and facilitating nucleophilic attack of Br⁻ to small steric resistance carbon atom, leading to the open-ring step, which is considered as rate-determining step of thermal-driven CCA. Finally, CO₂ adsorbed on Lewis basic sites S²⁻ inserted into the open-ring product to complete ring closure. On the other hand, Wannier carrier would be dissociated to generate photo-generated hole as well as electron under light excitation. photoinduced hole facilitates the coordination and polarization of adsorbed PO, Simultaneously, photoinduced electron would transfer to PO molecule to form electron-rich transition state, which was not only facilitate to the open-ring step of PO, but also greatly help the activation of CO₂ adsorbed adjacent S²⁻ sites. It should be noted that such electron-rich transition state is absence in above thermocatalysis. This is the most important difference between thermocatalysis and thermal_{Joule}-Photo-synergistic catalysis for such reaction in essence.

4. Conclusion

In summary, ZnIn₂S₄ with highly exposed Zinc sites were fabricated with solvothermal methods and utilized as thermal-photo_{nonthermal} (blue



Scheme1. Proposed Thermal-photo_{nonthermal}-synergistic catalytic mechanism of CO₂ cycloaddition on ZISE.

LED)-catalyst for CO₂ cycloaddition in consideration of Lewis acidity of Zinc cation as well as suitable light absorption ability. The optimized ZISE exhibits superior performance under blue LED illumination at 80 °C with TBAB for 8 h (Con 92.3%; Sel >99; 137.1 mmol/g/h), which is 4.40 times larger than pristine TBAB/dark system. Excitingly, it is 1.7 times higher than that without blue light under the same conditions, highlighting the necessary role of photocatalysis. The thermal-photo_{nonthermal}-synergistic catalysis activity of ZISE exceeds most of the reported catalytic. The broad substrate scope as well as robust recycling stability guarantee the potential and applicability of catalyst for CCA reaction. The E_a significantly decreases from 36.2 of thermocatalysis to 22.7 kJ·mol⁻¹ of thermal-photo_{nonthermal}-synergistic catalysis. On the other hand, ZISE with abundant of highly exposed Zinc sites facilitates physical and chemisorption of CO₂, which was beneficial for CO₂ adsorption and activation. The electron-rich transition state of thermal-photo_{nonthermal}-synergistic catalysis formed by the interaction of excited ZISE with PO molecules is the biggest difference from thermalcatalysis.

CRedit authorship contribution statement

Yuning Wu: Experiments, Data analysis & curation, Formal analysis, Writing – original draft. **Xue-Fang Yu:** Theoretical computations. **Yujie Du:** Data curation, Writing – review & editing. **Linhong Xia:** Investigation, Writing – review & editing. **Qi Guo:** Formal analysis, Writing – review & editing. **Kaisheng Zhang:** Resources, Methodology, Writing – review & editing. **Weilong Zhang:** Resources, Writing – review & editing. **Senmiao Liu:** Writing – review & editing. **Yanhua Peng:** Formal analysis, Writing – review & editing. **Zhuo Li:** Methodology, Formal analysis, Writing – review & editing. **Xiaolong Yang:** Conceptualization, Methodology, Formal analysis, Funding acquisition, Supervision, Writing – review & editing.

Declaration of Competing Interest

The authors declare that they have no known competing financial interests or personal relationships that could have appeared to influence the work reported in this paper.

Data Availability

Data will be made available on request.

Acknowledgement

We appreciate financial support from Natural Science Foundation of Shandong Province, China (ZR2019BB044); the National Key Research Development Program of China “Technology Boosts Economy 2020”, the State Key Research Development Program of China (2019YFC0408505); NSFC (21976182); Natural Science Foundation of Anhui Province (2008085 MB48); Qingdao University Innovation and entrepreneurship training program for College Students (X2022110650232). We also thank Shiyanjia Lab (www.shiyanjia.com) for characterizations.

Appendix A. Supporting information

Supplementary data associated with this article can be found in the online version at [doi:10.1016/j.apcatb.2023.122732](https://doi.org/10.1016/j.apcatb.2023.122732).

References

- H. Lin, S. Luo, H. Zhang, J. Ye, Toward solar-driven carbon recycling, *Joule* 6 (2022) 294–314.
- V.B.Y. Oh, S.F. Ng, W.J. Ong, Shining light on ZnIn₂S₄ photocatalysts: promotional effects of surface and heterostructure engineering toward artificial photosynthesis, *EcoMat* 4 (2022), e12204.
- P. Chen, Xa Dong, M. Huang, K. Li, L. Xiao, J. Sheng, S. Chen, Y. Zhou, F. Dong, Rapid self-decomposition of g-C₃N₄ during gas–solid photocatalytic CO₂ reduction and its effects on performance assessment, *ACS Catal.* 12 (2022) 4560–4570.
- P. Chen, B. Lei, Xa Dong, H. Wang, J. Sheng, W. Cui, J. Li, Y. Sun, Z. Wang, F. Dong, Rare-earth single-atom La-N charge-transfer bridge on carbon nitride for highly efficient and selective photocatalytic CO₂ reduction, *ACS Nano* 14 (2020) 15841–15852.
- B. pan, L. Zhou, J. Qin, M. Liao, C. Wang, Modulating CoFeOX Nanosheets Towards Enhanced CO₂ Photoreduction to Syngas: Effect of Calcination Temperature and Mixed-Valence Multi-Metals, *Chemistry-A European Journal*, 28 (2022) e202201992.
- H. Sugimoto, S. Inoue, Copolymerization of carbon dioxide and epoxide, *J. Polym. Sci. Part A: Polym. Chem.* 42 (2004) 5561–5573.
- J.-Q. Wang, K. Dong, W.-G. Cheng, J. Sun, S.-J. Zhang, Insights into quaternary ammonium salts-catalyzed fixation carbon dioxide with epoxides, *Catal. Sci. Technol.* 2 (2012) 1480–1484.
- R.R. Shaikh, S. Pornpraprom, V. D’Elia, Catalytic strategies for the cycloaddition of pure, diluted, and waste CO₂ to epoxides under ambient conditions, *ACS Catal.* 8 (2017) 419–450.
- J. Albero, Y. Peng, H. García, Photocatalytic CO₂ reduction to C₂+ products, *ACS, ACS Catal.* 10 (2020) 5734–5749.
- G. Zhai, Y. Liu, Y. Mao, H. Zhang, L. Lin, Y. Li, Z. Wang, H. Cheng, P. Wang, Z. Zheng, Y. Dai, B. Huang, Improved photocatalytic CO₂ and epoxides cycloaddition via the synergistic effect of Lewis acidity and charge separation over Zn modified UiO-bpydc, *Appl. Catal. B: Environ.* 301 (2022), 120793.
- L. Liu, J. Zhang, X. Cheng, M. Xu, X. Kang, Q. Wan, B. Han, N. Wu, L. Zheng, C. Ma, Amorphous NH₂-MIL-68 as an efficient electro- and photo-catalyst for CO₂ conversion reactions, *Nano Res.* (2022), <https://doi.org/10.1007/s12274-12022-14664-12270>.
- Q. Yang, C.C. Yang, C.H. Lin, H.L. Jiang, Metal-organic-framework-derived hollow N-doped porous carbon with ultrahigh concentrations of single Zn atoms for efficient carbon dioxide conversion, *Angew. Chem. Int. Ed.* 58 (2019) 3511–3515.
- G. Zhai, Y. Liu, L. Lei, J. Wang, Z. Wang, Z. Zheng, P. Wang, H. Cheng, Y. Dai, B. Huang, Light-promoted CO₂ conversion from epoxides to cyclic carbonates at ambient conditions over a Bi-based metal–organic framework, *ACS Catal.* 11 (2021) 1988–1994.
- Q. Yang, H. Peng, Q. Zhang, X. Qian, X. Chen, X. Tang, S. Dai, J. Zhao, K. Jiang, Q. Yang, J. Sun, L. Zhang, N. Zhang, H. Gao, Z. Lu, L. Chen, Atomically dispersed high-density Al-N₄ sites in porous carbon for efficient photodriven CO₂ cycloaddition, *Adv. Mater.* 33 (2021) 2103186.
- Y. Liu, Y. Chen, Y. Liu, Z. Chen, H. Yang, Z. Yue, Q. Fang, Y. Zhi, S. Shan, Zn and N co-doped porous carbon nanosheets for photothermally-driven CO₂ cycloaddition, *J. Catal.* 407 (2022) 65–76.
- F. Tang, L. Wang, L. Ma, Y. Fang, J. Huang, Y.-N. Liu, Protein-Zn(II) networks derived N-doped porous carbon-supported ZnS for photothermally catalytic CO₂ conversion, *J. CO₂ Util.* 45 (2021), 101431.
- W. Dai, M. Zou, J. Long, B. Li, S. Zhang, L. Yang, D. Wang, P. Mao, S. Luo, X. Luo, Nanoporous N-doped Carbon/ZnO hybrid derived from zinc aspartate: an acid-base bifunctional catalyst for efficient fixation of carbon dioxide into cyclic carbonates, *Appl. Surf. Sci.* 540 (2021), 148311.
- Y. Guo, L. Feng, C. Wu, X. Wang, X. Zhang, Confined pyrolysis transformation of ZIF-8 to hierarchically ordered porous Zn-N-C nanoreactor for efficient CO₂ photoconversion under mild conditions, *J. Catal.* 390 (2020) 213–223.
- Y. Pan, X. Yuan, L. Jiang, H. Yu, J. Zhang, H. Wang, R. Guan, G. Zeng, Recent advances in synthesis, modification and photocatalytic applications of micro/nano-structured zinc indium sulfide, *Chem. Eng. J.* 354 (2018) 407–431.
- Q. Zhu, Q. Xu, M. Du, X. Zeng, G. Zhong, B. Qiu, J. Zhang, Recent progress of metal sulfide photocatalysts for solar energy conversion, *Adv. Mater.* 34 (2022) 2202929.
- B. Pan, Y. Wu, B. Rhimi, J. Qin, Y. Huang, M. Yuan, C. Wang, Oxygen-doping of ZnIn₂S₄ nanosheets towards boosted photocatalytic CO₂ reduction, *J. Energy Chem.* 57 (2021) 1–9.
- J. Qin, Q. Zhao, Y. Zhao, Y. Wu, B. Pan, C. Wang, Metal-free phosphorus-doped ZnIn₂S₄ nanosheets for enhanced photocatalytic CO₂ reduction, *J. Phys. Chem. C* 125 (2021) 23813–23820.
- X. Jiao, Z. Chen, X. Li, Y. Sun, S. Gao, W. Yan, C. Wang, Q. Zhang, Y. Lin, Y. Luo, Y. Xie, Defect-mediated electron-hole separation in one-unit-cell ZnIn₂S₄ layers for boosted solar-driven CO₂ reduction, *J. Am. Chem. Soc.* 139 (2017) 7586–7594.
- Y. He, H. Rao, K. Song, J. Li, Y. Yu, Y. Lou, C. Li, Y. Han, Z. Shi, S. Feng, 3D hierarchical ZnIn₂S₄ nanosheets with rich Zn vacancies boosting photocatalytic CO₂ reduction, *Adv. Funct. Mater.* 29 (2019) 1905153.
- C. Feng, X. Yang, Z. Sun, J. Xue, L. Sun, J. Wang, Z. He, J. Yu, Dual interfacial synergism in Au-Pd/ZnIn₂S₄ for promoting photocatalytic selective oxidation of aromatic alcohol, *Appl. Surf. Sci.* 501 (2020), 144018.
- E. Zhang, Q. Zhu, J. Huang, J. Liu, G. Tan, C. Sun, T. Li, S. Liu, Y. Li, H. Wang, X. Wan, Z. Wen, F. Fan, J. Zhang, K. Ariga, Visually Resolving the Direct Z-Scheme Heterojunction in CdS@ZnIn₂S₄ Hollow Cubes for Photocatalytic Evolution of H₂ and H₂O₂ from Pure Water, *Applied Catalysis B: Environmental*, (2021) 120213.
- Y. Wu, H. Wang, W. Tu, S. Wu, J.W. Chew, Effects of composition faults in ternary metal chalcogenides (Zn_xIn₂S_{3+x}, x = 1–5) layered crystals for visible-light-driven catalytic hydrogen generation and carbon dioxide reduction, *Appl. Catal. B: Environ.* 256 (2019), 117810.
- B. Sun, J. Bu, X. Chen, D. Fan, S. Li, Z. Li, W. Zhou, Y. Du, In-situ interstitial zinc doping-mediated efficient charge separation for ZnIn₂S₄ nanosheets visible-light photocatalysts towards optimized overall water splitting, *Chem. Eng. J.* 435 (2022), 135074.

- [29] J. Qiu, L. Zhang, D. Dai, G. Xia, J. Yao, Cellulose-derived carbon dot-guided growth of ZnIn_2S_4 nanosheets for photocatalytic oxidation of 5-Hydroxymethylfurfural into 2,5-Diformylfuran, *ChemSusChem* 15 (2022), e202200399.
- [30] S. Mao, J.-W. Shi, G. Sun, D. Ma, C. He, Z. Pu, K. Song, Y. Cheng, Au nanodots@thiol-UiO66@ ZnIn_2S_4 nanosheets with significantly enhanced visible-light photocatalytic H_2 evolution, *Eff. Differ. Au Positions Transf. Electron-hole pairs*, *Appl. Catal. B: Environ.* 282 (2021), 119550.
- [31] C. Du, B. Yan, G. Yang, Promoting photocatalytic hydrogen evolution by introducing hot islands: SnSe nanoparticles on ZnIn_2S_4 monolayer, *Chem. Eng. J.* 404 (2021), 126477.
- [32] Y. Zhao, Y. Chen, L. Du, Q. Wang, X. Liu, L. Li, G. Tian, Fabrication of size-controlled hierarchical $\text{ZnS@ZnIn}_2\text{S}_4$ heterostructured cages for enhanced gas-phase CO_2 photoreduction, *J. Colloid Interface Sci.* 605 (2022) 253–262.
- [33] L. Xia, Z. Sun, Y. Wu, X.-F. Yu, J. Cheng, K. Zhang, S. Sarina, H.-Y. Zhu, H. Weerathunga, L. Zhang, J. Xia, J. Yu, X. Yang, Leveraging doping and defect engineering to modulate exciton dissociation in graphitic carbon nitride for photocatalytic elimination of marine oil spill, *Chem. Eng. J.* 439 (2022), 135668.
- [34] A. Sabbah, I. Shown, M. Qorbani, F.-Y. Fu, T.-Y. Lin, H.-L. Wu, P.-W. Chung, C.-I. Wu, S.R.M. Santiago, J.-L. Shen, K.-H. Chen, L.-C. Chen, Boosting photocatalytic CO_2 reduction in a $\text{ZnS/ZnIn}_2\text{S}_4$ heterostructure through strain-induced direct Z-scheme and a mechanistic study of molecular CO_2 interaction thereon, *Nano Energy* 93 (2022), 106809.
- [35] M. Li, J. Su, L. Guo, Preparation and characterization of ZnIn_2S_4 thin films deposited by spray pyrolysis for hydrogen production, *Int. J. Hydrog. Energy* 33 (2008) 2891–2896.
- [36] S. Meng, C. Chen, X. Gu, H. Wu, Q. Meng, J. Zhang, S. Chen, X. Fu, D. Liu, W. Lei, Efficient photocatalytic H_2 evolution, CO_2 reduction and N_2 fixation coupled with organic synthesis by cocatalyst and vacancies engineering, *Appl. Catal. B: Environ.* 285 (2021), 119789.
- [37] Q. Luan, X. Xue, R. Li, L. Gu, W. Dong, D. Zhou, X. Wang, B. Li, G. Wang, C. Hou, Boosting photocatalytic hydrogen evolution: orbital redistribution of ultrathin ZnIn_2S_4 nanosheets via atomic defects, *Appl. Catal. B: Environ.* 305 (2022), 121007.
- [38] J. Xiong, X. Li, J. Huang, X. Gao, Z. Chen, J. Liu, H. Li, B. Kang, W. Yao, Y. Zhu, $\text{CN}_2\text{rGO@BPQDs}$ high-low junctions with stretching spatial charge separation ability for photocatalytic degradation and H_2O_2 production, *Appl. Catal. B: Environ.* 266 (2020), 118602.
- [39] P. Jin, L. Wang, X. Ma, R. Lian, J. Huang, H. She, M. Zhang, Q. Wang, Construction of hierarchical $\text{ZnIn}_2\text{S}_4\text{@PCN-224}$ heterojunction for boosting photocatalytic performance in hydrogen production and degradation of tetracycline hydrochloride, *Appl. Catal. B: Environ.* 284 (2021).
- [40] S. Li, C. Wang, Y. Liu, B. Xue, W. Jiang, Y. Liu, L. Mo, X. Chen, Photocatalytic degradation of antibiotics using a novel $\text{Ag/Ag}_2\text{S/Bi}_2\text{MoO}_6$ plasmonic p-n heterojunction photocatalyst: Mineralization activity, degradation pathways and boosted charge separation mechanism, *Chem. Eng. J.* 415 (2021), 128991.
- [41] D. Zhou, X. Xue, X. Wang, Q. Luan, A. Li, L. Zhang, B. Li, W. Dong, G. Wang, C. Hou, Ni, In co-doped ZnIn_2S_4 for efficient hydrogen evolution: modulating charge flow and balancing H adsorption/desorption, *Appl. Catal. B: Environ.* 310 (2022), 121337.
- [42] P.K. Prajapati, A. Kumar, S.L. Jain, First photocatalytic synthesis of cyclic carbonates from CO_2 and epoxides using CoPc/TiO_2 hybrid under mild conditions, *ACS Sustain. Chem. Eng.* 6 (2018) 7799–7809.
- [43] C. Liu, H. Niu, D. Wang, C. Gao, A. Said, Y. Liu, G. Wang, C.-H. Tung, Y. Wang, S-Scheme Bi-oxide/Ti-oxide molecular hybrid for photocatalytic cycloaddition of carbon dioxide to epoxides, *ACS Catal.* (2022) 8202–8213.
- [44] Z. Qin, H. Li, X. Yang, L. Chen, Y. Li, K. Shen, Heterogenizing homogeneous cocatalysts by well-designed hollow MOF-based nanoreactors for efficient and size-selective CO_2 fixation, *Appl. Catal. B: Environ.* 307 (2022), 121163.
- [45] A. Kumar, S. Samanta, R. Srivastava, Graphitic carbon nitride modified with Zr-thiamine complex for efficient photocatalytic CO_2 insertion to epoxide: comparison with traditional thermal catalysis, *ACS Appl. Nano Mater.* 4 (2021) 6805–6820.
- [46] Q. Shao, S. Wei, X. Hu, H. Dong, T. Wen, L. Gao, C. Long, Tuning the micro-coordination environment of Al in dealumination Y zeolite to enhance electron transfer at the Cu-Mn oxides interface for highly efficient catalytic ozonation of toluene at low temperatures, *Environ. Sci. Technol.* 56 (2022) 15449–15459.
- [47] K. Yu, P. Puthiaraj, W.-S. Ahn, One-pot catalytic transformation of olefins into cyclic carbonates over an imidazolium bromide-functionalized Mn(III)-porphyrin metal-organic framework, *Appl. Catal. B: Environ.* 273 (2020), 119059.
- [48] Y. Li, G. Zhai, Y. Liu, Z. Wang, P. Wang, Z. Zheng, H. Cheng, Y. Dai, B. Huang, Synergistic effect between boron containing metal-organic frameworks and light leading to enhanced CO_2 cycloaddition with epoxides, *Chem. Eng. J.* 437 (2022), 135363.
- [49] G. Huang, Q. Niu, Y. He, J. Tian, M. Gao, C. Li, N. An, J. Bi, J. Zhang, Spatial confinement of copper single atoms into covalent triazine-based frameworks for highly efficient and selective photocatalytic CO_2 reduction, *Nano Res.* 15 (2022) 8001–8009.
- [50] F. Tang, L. Wang, L. Ma, Y. Fang, J. Huang, Y.-N. Liu, Protein-Zn(II) networks derived N-doped porous carbon-supported ZnS for photothermally catalytic CO_2 conversion, *J. CO_2 Util.* 45 (2021).
- [51] W. Dai, M. Zou, J. Long, B. Li, S. Zhang, L. Yang, D. Wang, P. Mao, S. Luo, X. Luo, Nanoporous N-doped Carbon/ ZnO hybrid derived from zinc aspartate: An acid-base bifunctional catalyst for efficient fixation of carbon dioxide into cyclic carbonates, *Appl. Surf. Sci.* 540 (2021), 148311.
- [52] A. Thomas, A. Fischer, F. Goettmann, M. Antonietti, J.-O. Müller, R. Schlögl, J. M. Carlsson, Graphitic carbon nitride materials: variation of structure and morphology and their use as metal-free catalysts, *J. Mater. Chem.* 18 (2008) 4893–4908.
- [53] Z. Fang, Z. Deng, X. Wan, Z. Li, X. Ma, S. Hussain, Z. Ye, X. Peng, Keggin-type polyoxometalates molecularly loaded in Zr-ferrocene metal organic framework nanosheets for solar-driven CO_2 cycloaddition, *Appl. Catal. B: Environ.* 296 (2021), 120329.
- [54] M. Bakiro, S. Hussein Ahmed, A. Alzamly, Efficient visible-light photocatalytic cycloaddition of CO_2 and propylene oxide using reduced graphene oxide supported BiNbO_4 , *ACS Sustain. Chem. Eng.* 8 (2020) 12072–12079.
- [55] L.G. Ding, B.J. Yao, W.X. Wu, Z.G. Yu, X.Y. Wang, J.L. Kan, Y.B. Dong, Metalloporphyrin and ionic liquid-functionalized covalent organic frameworks for catalytic CO_2 cycloaddition via visible-light-induced photothermal conversion, *Inorg. Chem.* 60 (2021) 12591–12601.
- [56] Q. Guo, S.G. Xia, X.B. Li, Y. Wang, F. Liang, Z.S. Lin, C.H. Tung, L.Z. Wu, Flower-like cobalt carbide for efficient carbon dioxide conversion, *Chem. Commun.* 56 (2020) 7849–7852.
- [57] J.F. Kurisingal, Y. Rachuri, Y. Gu, Y. Choe, D.-W. Park, Multi-variate metal organic framework as efficient catalyst for the cycloaddition of CO_2 and epoxides in a gas-liquid-solid reactor, *Chem. Eng. J.* 386 (2020), 121700.